Model Tests of a TLP Floating Offshore Wind Turbine with a Porous Outer Column

Ed Mackay, Lars Johanning
College of Engineering, Maths & Physical Science, University of Exeter, Penryn, UK

Wei Shi, Dezhi Ning
State Key Laboratory of Coastal and Offshore Engineering, Dalian University of Technology, Dalian, China

ABSTRACT

This paper presents the results of scaled model tests of a tension leg platform (TLP) for a floating wind turbine, comprising a central solid cylinder with a porous outer cylinder. Tests were conducted with outer cylinders with porosities of 0%, 15% and 30% and compared to a base case with no outer cylinder. For each configuration, the total mass and centre of mass are kept constant to allow consistent comparison. It is shown that for the cases with a solid outer cylinder the surge motion resonance is shifted to a lower frequency due to the entrained mass of water inside and increased added mass of the outer cylinder. Increasing the porosity of the outer cylinder is shown to increase the frequency of the resonant response, bringing the resonant frequency closer to that of the base case with no outer cylinder. Increasing the porosity of the outer cylinder also reduces the amplitude of the resonant response. The use of a porous outer layer increases the quadratic drag on the body and significantly reduces the low frequency resonant response where the radiation damping is low.

KEY WORDS: Renewable Energy; Floating Offshore Wind Turbine; Motion Damping; Hydrodynamic Response.

INTRODUCTION

A key challenge for developing cost-competitive floating offshore wind is the efficient design of stable platforms. Large platform motions can lead to reduced energy yield and increased fatigue loads on the turbine. Adding a porous outer layer to a floating platform has the potential to reduce platform motions without significant increase in size and cost.

Porous structures are commonly used in fixed and floating breakwaters to dissipate wave energy and reduce wave disturbance (e.g. Huang et al, 2011; Dai et al, 2018). The use of porous structures has also been investigated for motion damping and load reduction on fixed offshore structures (e.g. Molin, 1990; Molin, 2011; Park et al, 2014) and floating structures (e.g. Downie et al, 2000a,b; Williams et al, 2000; Lee & Kerr, 2002; Park et al, 2013; Vijay & Sahoo, 2018).

In this work, we present the results of scaled model tests of a tension leg platform (TLP) for a floating wind turbine, where the TLP is tested with various solid and porous outer cylinders. The purpose of the tests was to gather empirical data on the motion response of the TLP, primarily for the purpose of validating numerical predictions from a boundary element model (Mackay et al, 2018). In the present paper we report the empirical findings and the numerical validation will be reported in future work. As the primary purpose of the model tests was to validate numerical predictions, the model was designed to provide simple validation cases rather than optimised performance. Using a TLP as the floating support structure means that motions can be restricted to a single degree of freedom (surge), with very little heave or pitch motion, which simplifies the analysis of the test data. This is particularly useful for analysing the quadratic drag that results from the flow through the porous outer cylinders.

The paper is organised as follows. Section 2 discusses potential scale effects relevant to Froude-scaled model tests involving porous structures. The model used is described in Section 3 and the mooring configuration is described in Section 4. An overview of the experimental setup and tests conducted is presented in Section 5 and results are presented in Section 6. Finally, conclusions are given in Section 7. Throughout the paper, all values are reported at model scale.

SCALE EFFECTS ON FLOW ACROSS A POROUS BARRIER

The pressure drop, ΔP, across a thin porous barrier can be modelled as (Sollitt and Cross, 1972)

$$\frac{\Delta P}{\rho} = \frac{\nu U_n}{l} + \frac{C_f}{2} U_n |U_n| + L \frac{\partial U_n}{\partial t} \tag{1}$$

where ρ is the fluid density, ν is the kinematic viscosity, U_n is the component of the velocity normal to the porous barrier (assumed to be the average velocity close to the barrier, rather than the flow speed through the openings), l is a length scale (related to wall thickness, hole size, etc.), C_f is a dimensionless friction or drag coefficient and L is a coefficient with dimension of length. The first term on the RHS of (1) is a viscous friction loss, the second term is a turbulent dissipation loss, the third term represents inertial effects due to acceleration of the flow through the openings. Sollitt and Cross (1972) noted that the linear

drag term is dominant at low Reynolds number flow and the quadratic term is dominant at high Reynolds number. The Reynolds numbers for wave interaction with thin porous structures are usually high enough that linear viscous forces can be neglected.

The quadratic drag and inertia coefficients are dependent on the Reynolds number, which can be written as

$$Re = KC \cdot \beta, \tag{2}$$

where KC is the Keulegan-Carpenter number and β is the frequency parameter, defined as

$$KC = \hat{U}T/s, \tag{3}$$

$$\beta = s^2/\nu T, \tag{4}$$

where T is the period of the oscillatory flow, $\hat{U}$ is the amplitude of the velocity and s is the spacing between the hole centres. The KC number remains constant under Froude scaling, whereas β varies as $k^{3/2}$ (assuming viscosity remains constant), where k is the Froude scale factor. The magnitude of the scale effects on the flow through the porous cylinder is therefore dependent on the sensitivity of the drag coefficient to changes in β. The present tests use a nominal scale factor of 1:50, meaning that β at model scale is 354 times smaller than at full scale. Numerous studies have shown that pressure drop across a porous barrier in oscillatory flow is much more sensitive to KC than β (see e.g. Tao & Dray, 2008; Li et al, 2013; Tian et al, 2017). However, the range of values of β investigated in these studies is significantly smaller than a factor of 354 between the smallest and largest. It is therefore not possible to state unequivocally that the scale effects will be negligible and further work will be required to investigate the potential impact.

MODEL OVERVIEW

The model is a nominally 1:50 scale TLP with the dimensions based on the NREL design (Koo et al, 2012; Goupee et al, 2014). The purpose of the tests was to measure the influence of the porous outer cylinders on the hydrodynamic response of the platform. It was therefore decided to simplify the tests by not including the aerodynamic or gyroscopic effects of the rotor or the flexibility of the tower, so that the hydrodynamic effects can be examined in isolation. The rotor and nacelle were represented using an equivalent mass at the top of the tower, with the height of the tower and mass of the rotor and nacelle based on the NREL 5 MW turbine design (Jonkman et al, 2009). The dimensions of the model are illustrated in Fig. 1 and the mass and volumetric properties are listed in Table 1.

The model is designed to be tested with changeable outer cylinders with various diameters and porosities (see Fig. 2). The outer cylinders used had porosities of $\tau = 0$, 15 and 30% (where the 0% case is included for reference). The perforations in the porous cylinders were arranged in a square grid, using a constant hole spacing of $s = 25$ mm between hole centres (see Fig. 2). The hole radius, r, is therefore related to the porosity and hole spacing by $\tau = \pi r^2/s^2$. The outer cylinders had a wall thickness of 2 mm and diameters of 222.8 mm and 302.4 mm, giving an integer number of holes around the circumference. Numerous studies have found that the porosity has the dominant effect on the pressure drop across a thin porous barrier in oscillatory flow, with the hole spacing and wall thickness having a much smaller effect (see e.g. Mackay et al, 2019). The ratios of the diameters of the outer and inner cylinders are approximately 1.6 and 2.2 for the smaller and larger outer cylinders respectively.

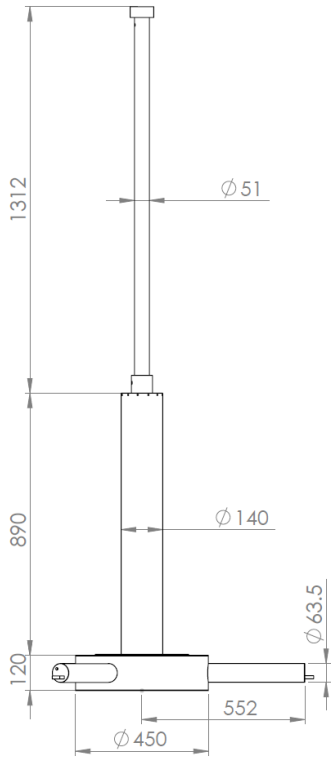

Fig. 1 Dimensions of base model (mm) with no outer cylinder.

To keep the total mass of the model constant between the various configurations, the inner cylinder contained a changeable mass, as shown in Fig. 2, which can be varied to compensate for the changes in the porosity and diameter of the outer cylinder. The masses were located half way up the column to maintain a constant centre of gravity (COG). In all seven configurations, the total mass of the model was 16.18 kg and the COG was 222 mm above the still water level. The pitch and roll moments of inertia did vary between model configurations. However, since the moorings were relatively stiff, there was very little motion in pitch and roll, with a maximum of less than 2° in the most extreme conditions and generally much less than 1°. The difference in the moments of inertia between configurations is therefore unlikely to influence the comparisons between configurations.

The model was designed to gather data for validation of numerical models and is not intended to give optimised performance. Both the inner cylinder and porous outer cylinders have a large, vertical freeboard to reduce non-linearities and avoid over-topping. It is also important to note that the model has been intentionally designed to resonate in surge at a frequency which can be excited in the tank, so that the influence of the porous outer cylinders can be measured.

Table 1 Model properties

Draft [mm]	600
Displaced volume [litre]	29.6
Mass [kg]	16.2
Vertical COG (rel. to MWL, positve upwards) [mm]	222

MOORING LINE PROPERTIES

The model was moored in a water depth of 1.2 m. The mooring comprises three vertical lines of 2 mm diameter Dyneema rope, attached to

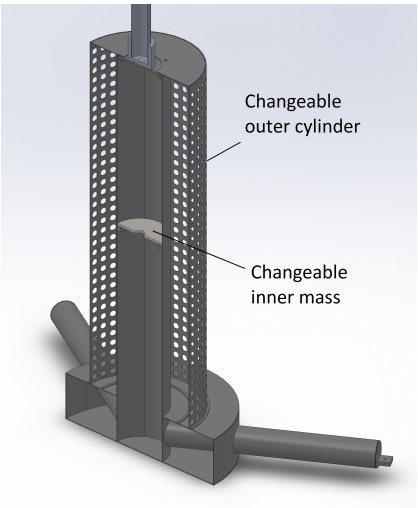

Fig. 2 Cross-section of model.

the ends of the legs and anchored to the tank floor. The locations of the attachment and anchor points are listed in Table 2, together with the axial stiffness (specified as a force per unit strain).

Table 2 Mooring line properties

Water depth [mm]	1200
Attachment point radius [mm]	567
Attachment point depth [mm]	647
Fairlead pivot height above tank floor [mm]	42
Mooring line length (pivot-pivot) [mm]	511
Mooring line axial stiffness [kN]	14.4

The horizontal restoring force for the model is the component of the mooring tension acting in the horizontal direction. The restoring force is slightly nonlinear due to the model moving in an arc and the resultant change in the buoyancy force with the horizontal displacement. To analyse the non-linearity of the restoring force we can consider a quasi-static analysis as follows. Define x to be the horizontal displacement of the model, L to be the initial length of the mooring line and T to be the mooring tension. Since the axial stiffness of the mooring lines is high, it is assumed that they are inextensible. The angle of the mooring lines to the vertical is $\theta = \sin^{-1}(x/L)$. The horizontal component of mooring force is

$$F_x = T \sin\theta = Tx/L. \tag{5}$$

The vertical component of the mooring force is

$$F_z = T \cos\theta = B - Mg, \tag{6}$$

where B is the buoyancy, M is the mass of the model and g is the acceleration due to gravity. The buoyancy is given by

$$B = \rho V g + sz, \tag{7}$$

where ρ is the density of water, V is the mean displaced volume, $s = \rho g A$ is the heave hydrostatic stiffness, A is the water-plane area and $z = L(1 - \cos\theta)$ is the vertical displacement. Substituting (7) into (6) and rearranging gives

$$T = (T_0 + zs)/\cos\theta, \tag{8}$$

where $T_0 = \rho V g - Mg$ is the pretension. Substituting this back into (5) gives

$$\begin{aligned} F_x &= (T_0 + sL(1 - \cos\theta))\tan\theta \\ &= T_0 \frac{x}{L} + (T_0 + sL)\left(\frac{1}{2}\left(\frac{x}{L}\right)^3 + \frac{3}{8}\left(\frac{x}{L}\right)^5 + \cdots\right), \end{aligned} \tag{9}$$

where the second expression is obtained by expressing z and $\tan\theta$ in terms of x and L and expanding as a Maclaurin series. The horizontal restoring force can be linearised to give

$$F_{x,Lin} = T_0 \frac{x}{L}. \tag{10}$$

The expressions above are compared to measurements during static displacement tests in Section 6.

EXPERIMENTS

The model was tested at the nonlinear wave flume at the State Key Laboratory of Coastal and Offshore Engineering, Dalian University of Technology. The flume is 60 m in length and 4 m in width and 2.5 m in depth, with a piston wavemaker at one end and a rubble/mesh beach at the other.

During the tests the model motions in 6 degrees of freedom (DOF) were measured using an infrared motion capture system (NDI Optotrak Certus®). As the tower was designed to be stiffer than an actual wind turbine tower, the model was treated as a single rigid body. The tension in each mooring line was measured using submersible inline load cells.

The following tests were conducted:

- Static offset
- Free decay
- Regular waves
- Unidirectional irregular waves

The regular wave tests comprised 25 tests at 13 frequencies and 3 amplitudes. All regular wave tests were run for 150 s. Six irregular wave conditions were tested (3 peak periods, T_p and two significant wave heights, H_s). Waves were generated from a JONSWAP spectrum with a peak enhancement factor $\gamma = 2$. The repeat time of the waves was 5 minutes and the tests were run for 5 min 30 s, and the initial 30 s ramp-up was discarded from the analysis. The wave conditions used are summarised in Tables 3 and 4.

All the wave conditions were measured without the model in the water using a linear array of wave probes, with one probe located at the undisturbed model position. The reflection coefficient was estimated using a 3-probe least squares method (Mansard & Funke, 1980) and was generally found to be less than 10% for wave frequencies above 0.35 Hz, but increased to around 40% for the two lowest frequency waves.

The amplitude of the response for the regular wave tests was estimated over a whole number of wave periods whilst both the waves and model were in steady state, after the initial transient had passed and the reflected waves had arrived back from the beach.

RESULTS AND DISCUSSION

Mooring response

The horizontal component of the mooring force (5) measured during the static displacement tests is plotted against surge in Fig. 3. The measured

Table 3 Regular wave conditions

Frequency [Hz]	Height [mm]
0.212	40, 80, 120
0.247	40
0.283	40, 80, 120
0.318	40
0.354	40, 80, 120
0.389	40
0.424	40, 80, 120
0.460	40
0.495	40, 80, 120
0.530	40
0.566	40, 80, 120
0.707	40
0.849	40

Table 4 Irregular wave conditions

T_p [s]	H_s [mm]
1.41	80, 160
1.70	80, 160
1.98	80, 160

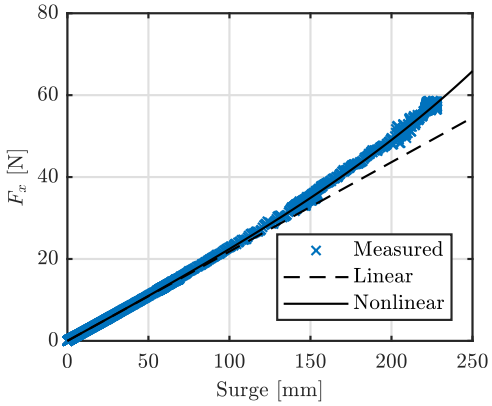

Fig. 3 Comparison of measured horizontal component of mooring force against static surge displacement with linear (10) and nonlinear models (9).

relationship is compared to the nonlinear expression (9) and the linear approximation (10). The measured horizontal force agrees very well with the nonlinear quasi-static model. The restoring force departs from the linear approximation by ~3% for a surge displacement of 100 mm and ~12% for a surge displacement of 200 mm.

Free decay

It is assumed that the equation of motion during the free decay tests can be written

$$(M + A)\ddot{x} + B\dot{x} + C|\dot{x}|\dot{x} + kx = 0, \tag{11}$$

where x is the surge position, M is the model mass, A is the added mass, B is a linear damping coefficient, C is a quadratic damping coefficient and k is the horizontal mooring stiffness. The mooring stiffness, k is known from the static displacement tests, described above. From the analysis in the previous section, the assumption of a linear restoring force is a good approximation for surge amplitudes less than 100 mm. The added mass can be estimated from the natural period using the relation $T_n = 2\pi\sqrt{(M + A)/k}$. The damping coefficients can be estimated from the data from the free decay test using the relation (Faltinsen, 1990):

$$\frac{2(M + A)}{T_n} \log\left(\frac{X_{m-1}}{X_{m+1}}\right) = B + \frac{16X_m}{3T_n}C \tag{12}$$

where T_n is the natural period and X_m is the amplitude of the m^{th} oscillation. Fig. 4 shows the LHS of (12) plotted against $16X_m/3T_n$ for the base configuration (no outer cylinder) and the three configurations with OD 223 mm, together with linear regression lines. The damping coefficients B and C are the intercept and gradient of the regression lines. The results for the cases with the larger outer cylinders exhibited similar trends and are not shown here. The natural periods, added mass and damping coefficients estimated from the decay tests are listed in Table 5.

For the cases with the solid outer cylinders, the entrained mass of water between the inner and outer cylinders is approximately 11.4 kg for the OD 223 mm cylinder and 27.0 kg for the OD 302 mm cylinder. The added mass in these cases is 32.3 kg and 58.0 kg respectively (including the entrained mass of water), compared with 12.0 kg for the base case. For the cases with 30% porosity, there is only a small increase in the added mass, much smaller than the entrained mass of water between the inner and outer cylinders. This indicates that the entrained water between the inner cylinder and porous outer cylinders does not significantly contributed to the added mass in these cases, since the water is able to pass through the porous outer cylinder with low impedance. For the cases with 15% porosity, the added mass is approximately half way between the cases solid and 30% porosity cases.

For the base case and the cases with solid outer cylinders, the linear damping is due to wave radiation and the quadratic drag is due to vortex shedding. We would expect to see the linear damping increase with the cylinder diameter, whilst the variation of the drag with the diameter of the upper cylinder (and hence KC number) is geometry-dependent. The results in Table 5 show that the linear damping increases for the OD 223 mm solid cylinder and the drag decreases. However, the linear damping is lower for the solid OD 302 mm cylinder than the OD 223 mm cylinder, which is contrary to expectations. This indicates that the estimated linear damping coefficients may not be completely reliable. For the solid cases, the value of ka at the natural period (where k is the wavenumber and a is the radius of the upper cylinder) is in the range 0.07-0.08. The surge radiation damping coefficient for a small vertical cylinder is proportional to $(ka)^2$ (Mei, 1983). Therefore, the radiation damping around the natural period is very low, making the estimation from decay tests less reliable. The assumption of a constant drag coefficient, C, will also affect the results, since the drag coefficient varies with the KC number, especially for small amplitudes. Nevertheless, Fig. 4 shows a reasonable linear trend for the larger amplitude oscillations, indicating that assuming a constant drag coefficient may be reasonable for the larger oscillations, where drag is more significant. The cases with solid outer cylinders showed reduced drag compared to the base case.

For the cases with 30% porosity, there is a strong linear trend in Fig. 4 over the full range of observations. However, the cases with 15% porosity have a steep gradient for smaller oscillations, which decreases for larger oscillations. In these cases the separation into linear and quadratic damping is less reliable. Despite this, it is clear that the damping for the 15% porosity cases is higher than for the cases with 30% porosity and significantly higher than for the cases with solid cylinders.

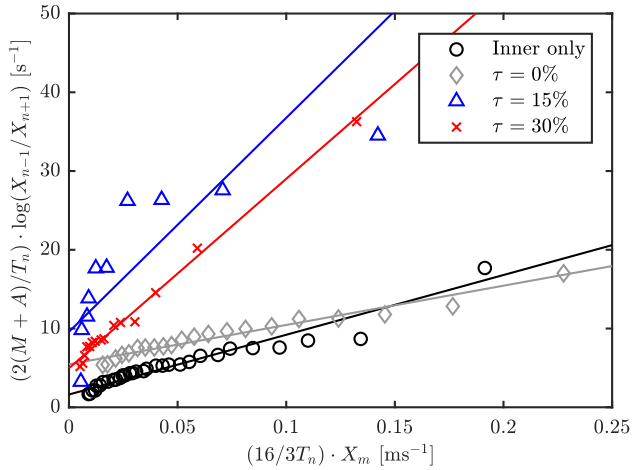

Fig. 4 Normalised logarithmic decrement against normalised amplitude from decay tests with outer cylinder diameter 223 mm. See (12) for details.

Table 5 Natural period, added mass and damping parameters from free decay tests

Outer cylinder diameter [mm]	Outer cyl. porosity [%]	T_n [s]	A [kg]	B [kg·s^{-1}]	C [kg·m^{-1}]
N/A	N/A	2.25	12.0	1.62	75.9
223	30	2.27	12.6	4.96	240.5
223	15	2.57	21.2	9.59	271.7
223	0	2.95	32.3	5.46	49.9
302	30	2.40	15.6	9.15	467.4
302	15	3.09	36.8	19.98	434.7
302	0	3.65	58.0	3.40	61.6

Regular wave response

The surge response amplitude operator (RAO) for the regular wave tests with H = 40 mm are shown in Fig. 5. The RAO for the base case with no outer cylinder has a peak value of 4.6 at a frequency of 0.42 Hz, close to the natural frequency found in the decay tests. There is an increased response for the lowest two frequencies. The response would be expected to decrease with frequency, so it is likely that the observed increase is due to the influence of reflected waves at these frequencies which were much higher than for the higher frequency waves. The increased response at the two lowest frequencies was observed for other configurations as well, indicating that it is a consistent effect due to the reflected waves.

The addition of a solid outer cylinder shifts the peak response to a lower frequency, due to the increased added mass. The amplitude of the peak response also increases with diameter of the outer cylinder, which is related to the decrease in radiation damping relative to the excitation force with frequency.

As the porosity of the outer cylinder is increased, the peak response reduces. The cases with 15% porosity are similar to the cases with solid outer cylinders, but with reduced peak response and a small increase in the response at higher frequencies. The cases with 30% porosity have a further reduction in the amplitude of the peak response, with the peak occurring at a frequency between that for the base case and the solid outer cylinder cases. The porous outer cylinders with the larger diameter give a larger reduction in the response, with the peak response of the cases with OD 302 mm and τ = 30% having a peak RAO of 2.7

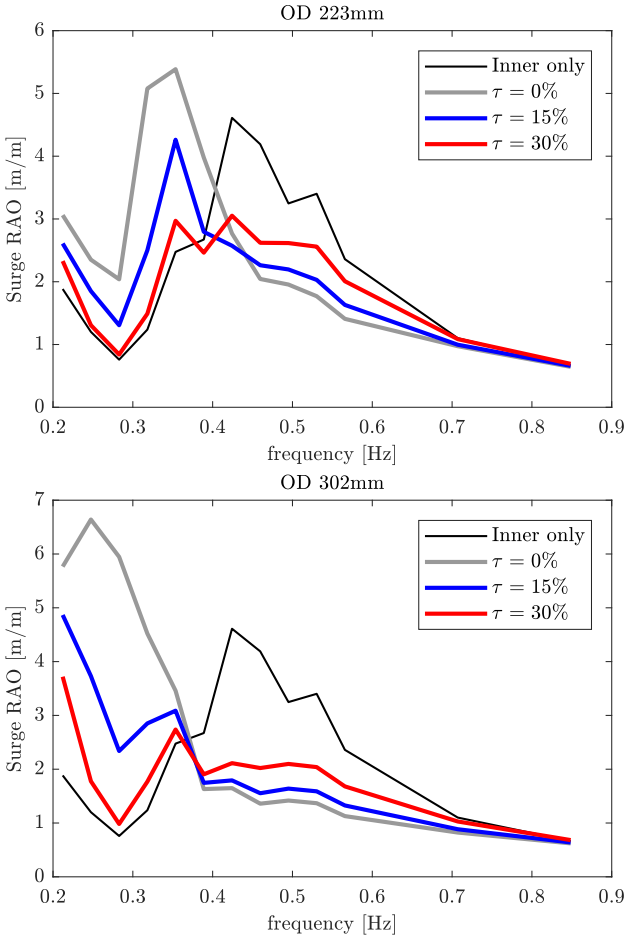

Fig. 5 Surge RAOs for the cases with outer cylinder OD 223 mm (upper plot) and OD 302 mm (lower plot). Both plots for tests with wave height H = 40 mm.

(ignoring the first two frequencies which are affected by reflections), a reduction of approximately 40%.

As the porous outer cylinders significantly increase the quadratic damping, it is interesting to examine the linearity of the response. The RAOs for each configuration at the three regular wave heights are shown in Fig. 6. For the base case (no outer cylinder) there is a significant reduction in the response for larger wave heights, due to the increased drag for the larger motions. The slight non-linearity in the mooring stiffness at larger amplitudes will tend to shift the peak response to higher frequencies, but this effect is not visible here. For the cases with porous outer cylinders, there is a smaller relative change. The case with OD 223 mm, τ = 15% shows a reduction in the peak response at higher amplitudes, whilst the case with OD 223 mm, τ = 30% has a small reduction in the response at the higher frequency end. The cases with OD 302 mm porous cylinders show a smaller change in the response with increasing wave height.

Irregular wave response

The wave spectra measured during the irregular wave tests are shown in Fig. 7. The spectra have been calculated over the repeat period of the waves and smoothed using a running mean over 25 harmonics. The corresponding surge response spectra are shown in Fig. 8 and 9 and have been processed in the same way. The response in irregular waves follows a similar pattern to the response in regular waves. The addition of the solid outer cylinder shifts the response to a lower

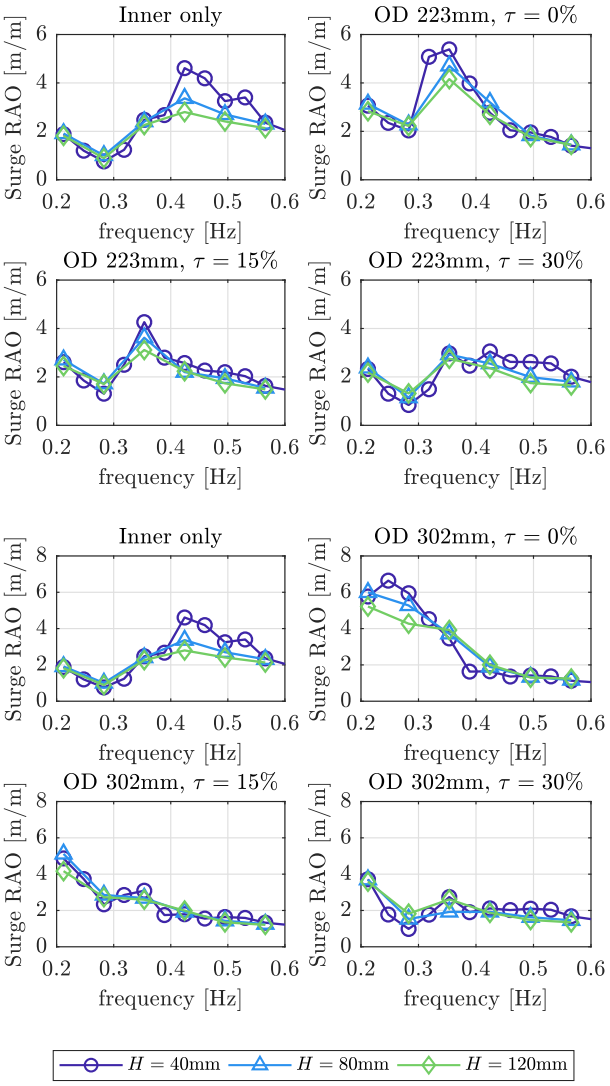

Fig. 6 Effect of wave height on surge RAOs for each case.

frequency and reduces the peak response at the natural period of the base configuration (no outer cylinder). The case with the solid outer cylinder OD 223 mm has an increased low frequency response compared to the base case. However, the case with the larger solid outer cylinder shows a small low frequency response, since its natural period is below the frequency at which there is significant energy in the wave spectrum. The cases with porous outer cylinders show a reduction in the peak response, but without the increased low frequency response. The cylinders with τ = 15% have a marginally lower response at frequencies above 0.5 Hz, but slightly higher response at lower frequencies. The larger porous outer cylinders give a greater reduction in response as there is a larger surface area used for motion damping.

The RAOs derived from the irregular wave tests using the smaller outer cylinders are shown in Fig. 10. The corresponding RAOs from the regular wave tests are overlaid. The RAOs for the irregular wave tests are only shown for the frequency range where the wave spectral density is greater than 10^{-4}m^{2}s (see Fig. 7), since the results are subject to large uncertainties outside this range. The regular and irregular RAOs are in good agreement in general. For the base case, the non-linearity around

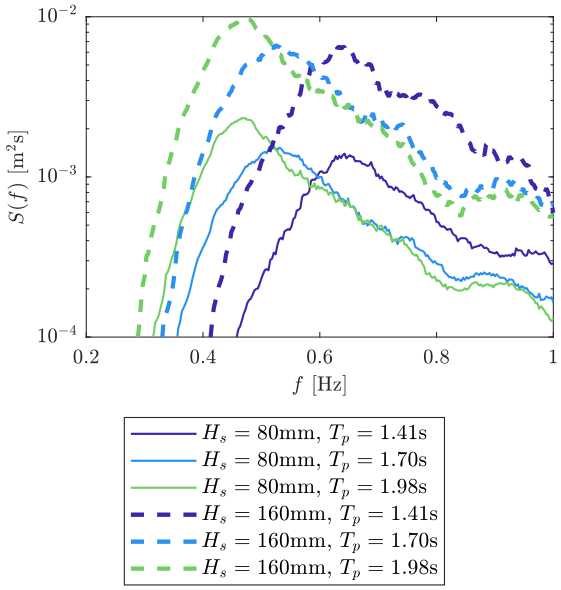

Fig. 7 Measured wave spectra for the six irregular wave cases.

the peak response is evident. It is not possible to directly compare results from the irregular and regular wave tests, since it is not possible to uniquely define the heights of the regular waves making up the spectrum (the regular heights depend on the frequency step at which the spectrum is discretised). However, it can be seen that the range of responses measured in the irregular wave tests are similar to those measured in the regular wave tests.

CONCLUSIONS

It has been shown that adding a porous outer cylinder to a floating structure can reduce the motion response by increasing the quadratic damping and shifting the resonance to a lower frequency by increasing the added mass. Using outer cylinders with a porosity of 30% resulted in very little change in the added mass compared to the base configuration with no outer cylinder, with the change in added mass much less than the entrained mass of water between the inner and outer cylinders. The added mass increases as the porosity decreases and the porous outer cylinder behaves more like a solid cylinder. The use of larger outer cylinders results in both higher damping due to the larger surface area involved and a larger shift in the resonant frequency due to the increase in added mass. The results indicate that the porosity and diameter of the outer cylinder could be tuned to optimise the natural frequency of the structure. The use of porous structures to damp low frequency resonant motions could be useful, since the radiation damping is small at low frequencies.

The test results showed that the response in irregular waves is similar to that in regular waves, indicating that frequency domain numerical calculations can be used to predict irregular wave response, despite the non-linearity introduced by the increased quadratic damping.

ACKNOWLEDGEMENT

We thank Dr Peter Halswell of the University of Exeter for assistance in designing the scale model. This work was funded through EPSRC (UK) grant for the project “Resilient Integrated-Coupled FOW platform design methodology (ResIn)” [grant number EP/R007519/1] and the National Natural Science Foundation of China [grant number 51761135011].

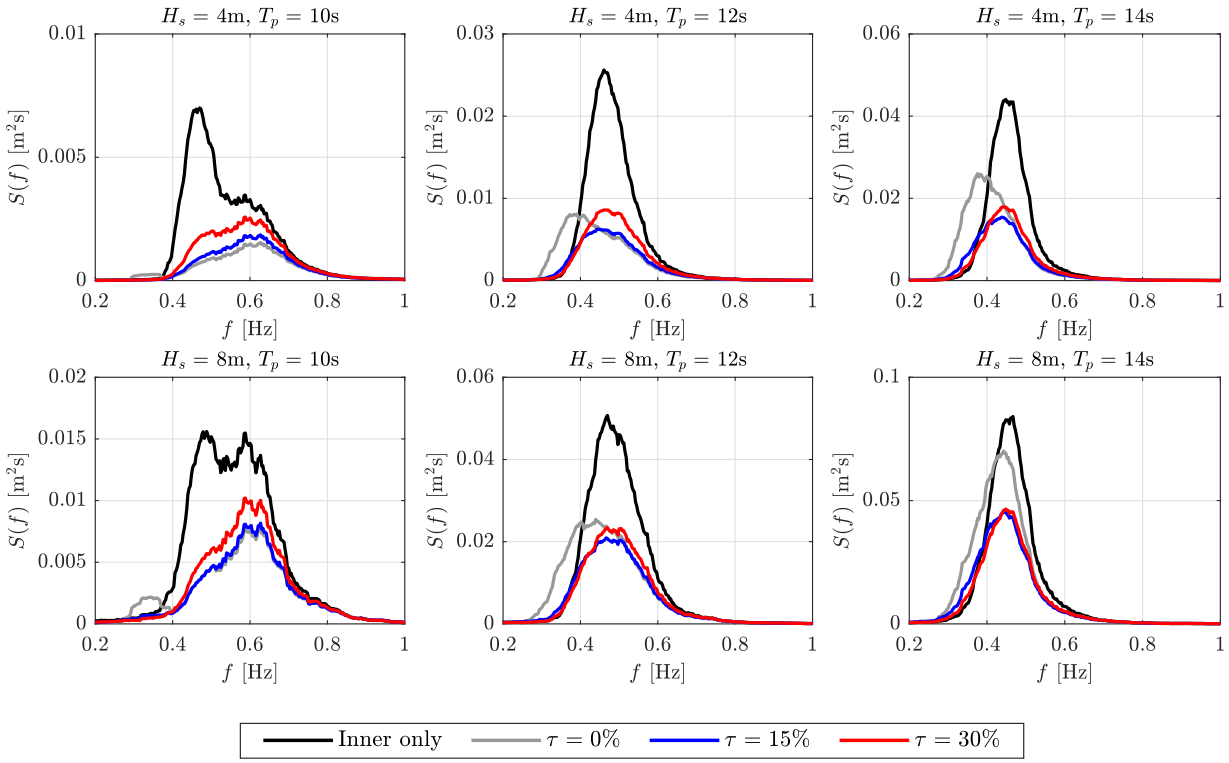

Fig. 8 Surge response spectra in the six irregular wave tests for outer cylinders OD 223 mm.

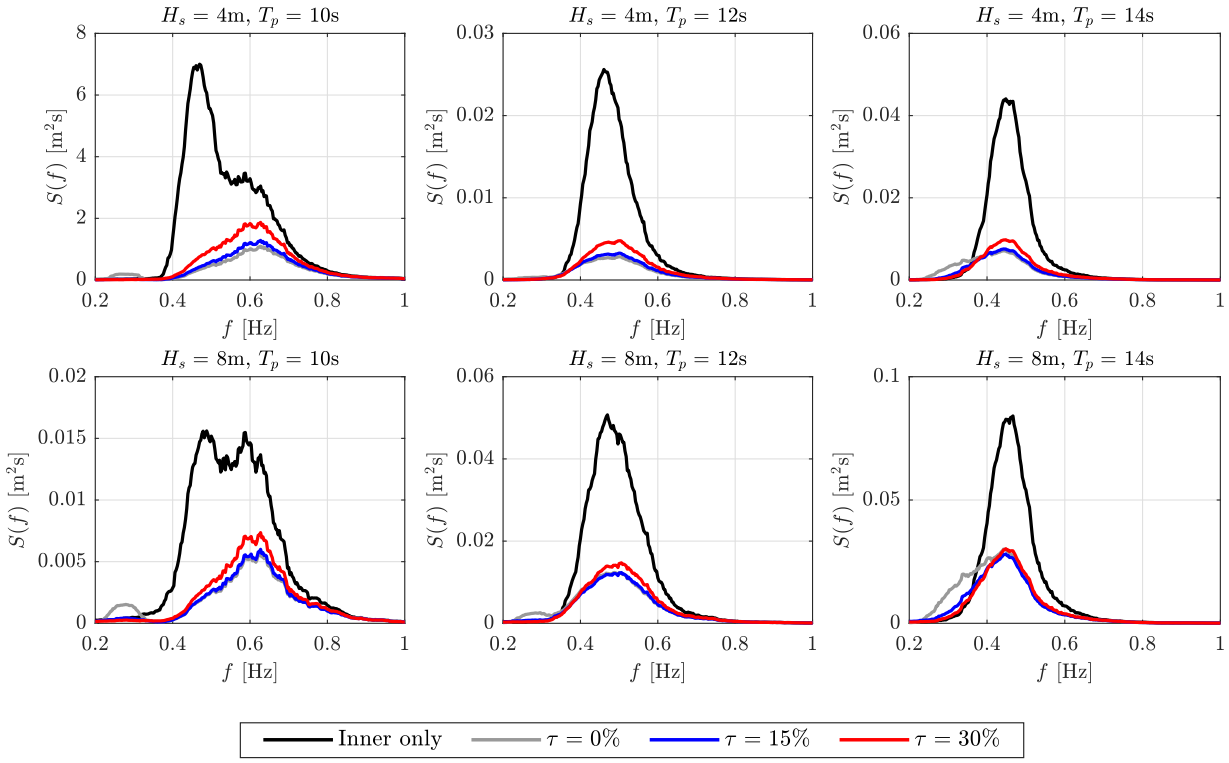

Fig. 9 Surge response spectra in the six irregular wave tests for outer cylinders OD 302 mm.

REFERENCES

J. Dai, C. M. Wang, T. Utsunomiya, and W. Duan. Review of recent research and developments on floating breakwaters. *Ocean Engineering*, 158:132–151, 2018.

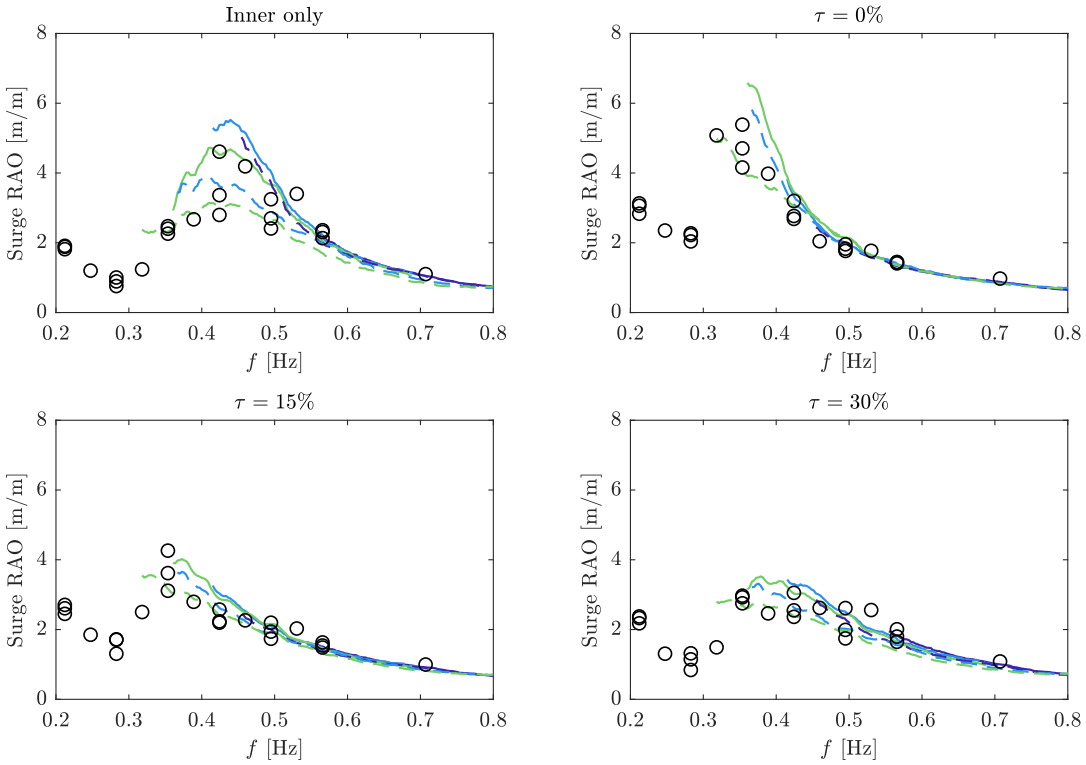

Fig. 10 Lines: RAOs from irregular wave tests with outer cylinders OD 223 mm (see Fig. 7 for legend). Circles: RAOs from regular wave tests.

M. Downie, J. Wang, and J. Graham. The Effectiveness of Porous Damping Devices. In *10th International Offshore and Polar Engineering Conference*, pages 418–425, 2000a.

M. J. Downie, J. M. Graham, C. Hall, A. Incecik, and I. Nygaard. An experimental investigation of motion control devices for truss spars. *Marine Structures*, 13:75–90, 2000b.

O. Faltinsen. *Sea Loads on Ships and Offshore Structures*. Cambridge University Press, 1990.

A. J. Goupee, B. J. Koo, R. W. Kimball, K. F. Lambrakos, and H. J. Dagher. Experimental comparison of three floating wind turbine concepts. *Journal of Offshore Mechanics and Arctic Engineering*, 136:1–9, 2014.

Z. Huang, Y. Li, and Y. Liu. Hydraulic performance and wave loadings of perforated / slotted coastal structures : A review. *Ocean Engineering*, 38(10):1031–1053, 2011.

J. Jonkman, S. Butterfield, W. Musial, and G. Scott. Definition of a 5-MW reference wind turbine for offshore system development. Technical report, National Renewable Energy Laboratory, 2009.

B. Koo, A. J. Goupee, K. Lambrakos, and R. W. Kimball. Model tests for a floating windturbine on three different floaters. In *31st International Conference on Offshore Mechanics and Arctic Engineering*, volume 7, pages OMAE2012–83642, 2012.

C. P. Lee and W. K. Ker. Coupling of linear waves and a hybrid porous TLP. *Ocean Engineering*, 29:1049–1066, 2002.

J. Li, S. Liu, M. Zhao, and B. Teng. Experimental investigation of the hydrodynamic characteristics of heave plates using forced oscillation. *Ocean Engineering*, 66:82–91, 2013.

E. Mackay, L. Johanning, D. Ning, and D. Qiao. Numerical and experimental modelling of wave loads on thin porous sheets. In *38th International Conference on Ocean, Offshore and Arctic Engineering*, pages 1–10, 2019.

E. B. Mackay, A. Feichtner, R. E. Smith, P. R. Thies, and L. Johanning. Verification of a boundary element model for wave forces on structures with porous elements. In *3rd International Conference on Renewable Energies Offshore, RENEW 2018*, pages 341–350, 2018.

Mansard EPD and F. ER. The measurement of incident and reflected spectra using a least squares method. In *17th Coastal Engineering Conference*, pages 154–172, 1980.

C. C. Mei. *The applied dynamics of ocean surface waves*. World Scientific, 1983.

B. Molin. Hydrodynamic modeling of perforated structures. *Applied Ocean Research*, 33(1):1–11, 2011.

B. Molin and J.-L. Legras. Hydrodynamic modeling of the Roseau tower stabilizer. In *9th OMAE conference*, pages 329–336, 1990.

M. S. Park, Y. J. Jeong, Y. J. You, and J. H. Park. Reliability evaluations of an offshore platform with partial porous cylinders due to wave and seismic forces. In *32nd International Conference on Offshore Mechanics and Arctic Engineering*, pages OMAE2013–10557, 2013.

M.-S. Park, Y.-J. Jeong, Y.-J. You, D.-H. Lee, and B.-C. Kim. Numerical analysis of a hybrid substructure for offshore wind turbines. *Journal of Civil Engineering and Architecture Research*, 1:230–238, 2014.

C. Sollitt and R. Cross. Wave transformation through permeable breakwaters. In *13th International Conference on Coastal Engineering*, pages 1827–1846, 1972.

L. Tao and D. Dray. Hydrodynamic performance of solid and porous heave plates. *Ocean Engineering*, 35(10):1006–1014, 2008.

X. Tian, L. Tao, X. Li, and J. Yang. Hydrodynamic coefficients of oscillating flat plates at 0.15 <= KC<= 3.15. *Journal of Marine Science and Technology (Japan)*, 22(1):101–113, 2017.

K. Vijay and T. Sahoo. Retrofitting of floating bridges with perforated outer cover for mitigating wave-induced responses. In *37th International Conference on Ocean, Offshore and Arctic Engineering*, pages OMAE2018–77054, 2018.

A. N. Williams, W. Li, and K. H. Wang. Water wave interaction with a floating porous cylinder. *Ocean Engineering*, 27:1–28, 2000.